


# Design and Modeling of a Compact Spooling Mechanism for the COAST Guidewire Robot

Timothy A. Brumfiel , *Graduate Student Member, IEEE*, Jared Grinberg , *Graduate Student Member, IEEE*, Betina Siopongco , and Jaydev P. Desai , *Fellow, IEEE*

**Abstract**—The treatment of many intravascular procedures begins with a clinician manually placing a guidewire to the target lesion to aid in placing other devices. Manually steering the guidewire is challenging due to the lack of direct tip control and the high tortuosity of vessel structures, potentially resulting in vessel perforation or guidewire fracture. These challenges can be alleviated through the use of robotically steerable guidewires that can improve guidewire tip control, provide force feedback, and, similar to commercial guidewires, are inherently safe due to their compliant structure. However, robotic guidewires are not yet clinically viable due to small robot lengths or large actuation systems. In this letter, we develop a highly compact spooling mechanism for the **CO**axially **A**ligned **ST**eerable (COAST) guidewire robot, capable of dispensing a clinically viable length of 1.5 m of the robotic guidewire. The mechanism utilizes a spool with several interior armatures to actuate each component of the COAST guidewire. The kinematics of the robotic guidewire are then modeled considering additional friction forces caused by interactions within the mechanism. The actuating mechanisms of the compact spooling mechanism are calibrated and the kinematics of the guidewire are validated resulting in an average curvature RMSE of  $0.24 \text{ m}^{-1}$ .

**Index Terms**—Medical robotics and systems, mechanism design, tendon/wire mechanism.

## I. INTRODUCTION

**C**ARDIOVASCULAR diseases (CVDs) are a group of disorders that affect the heart and blood vessels that take approximately 17.9 million lives each year, globally [1]. In the United States alone, CVDs remain the leading cause of death with approximately 49.2% of adults being affected by them [2]. Treatment of these conditions often begins with a skilled clinician manually steering a slender rod, called a guidewire, to the target locations in the vasculature. Guidewires provide a

path for larger devices, such as catheters, to the desired location in the body. These wires are typically made of stainless steel or super-elastic nitinol (NiTi) with diameters in the range of 0.008”–0.038” (0.2 mm–0.89 mm) with standard lengths of 150 cm and 350 cm. The navigation of guidewires, however, is challenging due to the high torsional and bending compliance of the guidewire and the lack of direct tip control. Consequently, clinicians and patients are exposed to radiation for longer periods, and the risk of vessel perforation or guidewire fracture, which can be fatal [3], is higher.

Continuum robots have increasingly been developed for use in minimally invasive procedures due to their inherent compliance, ability to follow complex trajectories using methods such as follow-the-leader motion [4], ability to provide contact force measurements from shape [5], [6], [7], [8], and high potential for miniaturization. These robots are typically tendon-driven [9], [10], [11], magnetically actuated [12], [13], [14], constructed from concentric pre-curved tubes [15], [16], [17], [18], or thermally actuated through shape memory alloys (SMAs) [19], [20]. These mechanisms are utilized to enable steering in a robotically steerable guidewire, but many of these methods are not currently feasible for enabling clinically viable lengths required for catheter and guidewire systems. Magnetically actuated guidewires use an inconvenient, bulky set-up that is difficult to use in the operating room. For example, the magnetic actuation system developed in [12] contained 8, 210 mm × 62 mm diameter electromagnets, a setup that is inconvenient in a clinical settings [21]. Additionally, the heating mechanisms that SMAs use to manipulate their shape could potentially damage tissue [22] and require complex cooling systems to perform with an acceptable bandwidth. These mechanisms also require the use of long, linear actuation system, an example of which is seen in [23] where a single SMA actuator developed had an overall dimension of 205 mm × 26 mm × 44 mm [23]. The work presented in [24] developed a handheld device with an overall dimension of 258 mm × 48 mm × 160 mm to actuate a concentric tube robot of up to 120 mm in length. These works demonstrate the lack of spatially compact actuation systems for clinically viable guidewire lengths.

Tendon-driven guidewires appear to be the most promising mechanism for compactness, but current approaches do not contain clinically viable lengths of robotic guidewires nor do they have a compact setup. In our previous works [25], [26], [27], robotically steerable guidewires were developed that utilized a linear motion stage. While the mechanism was compact in

Received 14 June 2024; accepted 13 August 2024. Date of publication 21 August 2024; date of current version 12 September 2024. This article was recommended for publication by Associate Editor Long Wang and Editor Jessica Burgner-Kahrs upon evaluation of the reviewers' comments. Research reported in this publication was supported in part by the National Heart, Lung, And Blood Institute of the National Institutes of Health under Award Number R01HL144714. The content is solely the responsibility of the authors and does not necessarily represent the official views of the National Institutes of Health. (Corresponding author: Timothy A. Brumfiel.)

Timothy A. Brumfiel and Jaydev P. Desai are with the Medical Robotics and Automation (RoboMed) Laboratory, Wallace H. Coulter Department of Biomedical Engineering, Georgia Institute of Technology, Atlanta, GA 30332 USA (e-mail: tbrumfiel3@gatech.edu).

Jared Grinberg and Betina Siopongco contributed to this work when they were with the RoboMed Laboratory at the Georgia Institute of Technology, Atlanta, GA 30332 USA (e-mail: grinberg.jared@gmail.com; betinasiopongco@gmail.com).

Digital Object Identifier 10.1109/LRA.2024.3447466

diameter, the length of the mechanism was 638.4 mm long and was only tested on guidewires up to a length of 242 mm. To address this major limitation, our work in [28] aimed to develop a compact spooling mechanism for a modified version of the COaxially Aligned STeerable (COAST) guidewire robot. This guidewire robot is capable of follow-the-leader (FTL) motion through a variable bending length and extended-feed (ExF) motion through a translating micromachined outer tube. This mechanism, however, was unable to include all three of the concentric tubes of the COAST guidewire robot and required a larger diameter NiTi tube as the bending joint. As a result, the robot was incapable of performing the motion profiles that the COAST guidewire robot was designed to achieve.

In this work, we develop a compact spooling mechanism that can dispense a clinically viable length of up to 150 cm of the COAST guidewire robot. The proposed mechanism is differentiated from the mechanism previously developed [28] in the following aspects:

- 1) The proposed mechanism (12 cm OD spool) houses and actuates each component of the COAST guidewire robot with minimal increase to the OD of the spool; The previous mechanism (10 cm OD spool) could only house a modified COAST guidewire with fewer degrees-of-freedom (DoF).
- 2) The proposed design incorporates a method for preventing the buckling of the sub-0.5 mm tubes while being actuated. This feature was not present in the previous mechanism. The aforementioned feature is integral to developing guidewires for procedures such as stroke, aneurysm coiling, cerebral embolization, as well as other tortuous anatomies.
- 3) The proposed mechanism incorporates features to enable all the unique capabilities of the COAST guidewire, such as FTL and ExF motion, to be fully utilized through the use of armatures that actuate each inner component of the COAST guidewire. Furthermore, these capabilities were realized while maintaining the overall size of the guidewire in the previous work [28].

In addition to presenting the design of the proposed mechanism, the kinematics of the COAST guidewire robot are extended to incorporate the effects of the spooling mechanism. The primary contributions of this work are:

- Design and joint space control of a highly compact spooling mechanism for the COAST guidewire robot.
- Modeling of friction caused by the components of the spooling mechanism into the kinematic model of the COAST guidewire robot to determine joint actuation required for a desired curvature.

The letter is organized as follows. In Section II, the COAST guidewire robot utilized in this work is introduced (Section II-A) with the compact spooling mechanism (Section II-B) and the kinematics of the guidewire (Section II-C) are presented. In Section III each component of the spooling mechanism is calibrated and validated (Section III-A) followed by a validation of the kinematics model of the guidewire (Section III-B). Lastly, conclusions and future work are presented in Section IV.

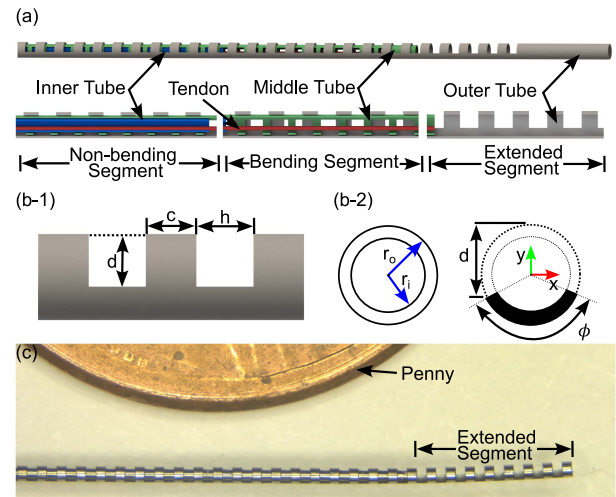


Fig. 1. A schematic of (a) the COAST guidewire robot with each segment, (b-1) the notch parameters defined for a UAN joint, and (b-2) the cross-sectional area of the UAN joint. An image of (c) the COAST guidewire is shown with a penny for scale.

## II. MATERIALS AND METHODS

### A. COAST Guidewire

The COAST guidewire utilized in this work consists of three coaxially aligned tubes: the inner tube, the middle tube, and the outer tube with an outer diameter (OD) of 0.26 mm, 0.36 mm, and 0.48 mm, respectively. Both the middle and outer tubes are superelastic NiTi tubes that are micromachined using a femtosecond laser (Optec Laser S.A., Frameries, Belgium) with a unidirectional asymmetric notch (UAN) pattern to allow for compliance in a single plane. Each notch pattern consists of  $N_{mid}$  and  $N_{out}$  rectangular notches for the middle and outer tubes, respectively. The middle and outer tubes can develop pre-curvatures due to the asymmetric heating that occurs during laser micromachining which can result in a non-zero combined tube pre-curvature [25]. To mitigate this, the middle and outer tubes are aligned with the notches 180° out-of-phase which can mostly eliminate the combined tube pre-curvature and reduce notch interactions while translating the tubes relative to one another. The inner tube of the COAST guidewire is a NiTi tube that has not been machined. Lastly, a NiTi micro-tendon with a 76  $\mu$ m OD (McMaster-Carr, USA) is routed through the inner tube and is terminated at the distal end of the middle tube by soldering it on the inner wall of the tube at the tip. The curvature of the middle tube can be changed by applying tension to the micro tendon. The complete structure of the COAST guidewire robot is shown in Fig. 1(a).

The COAST guidewire contains three separated segments, the non-bending segment, the bending segment, and the extended segment. The non-bending segment consists of all three tubes coaxially aligned. The combined stiffness of all three tubes prevents bending from occurring throughout this segment. The bending segment consists only of the laser micromachined middle and outer tubes. The length of the bending segment can

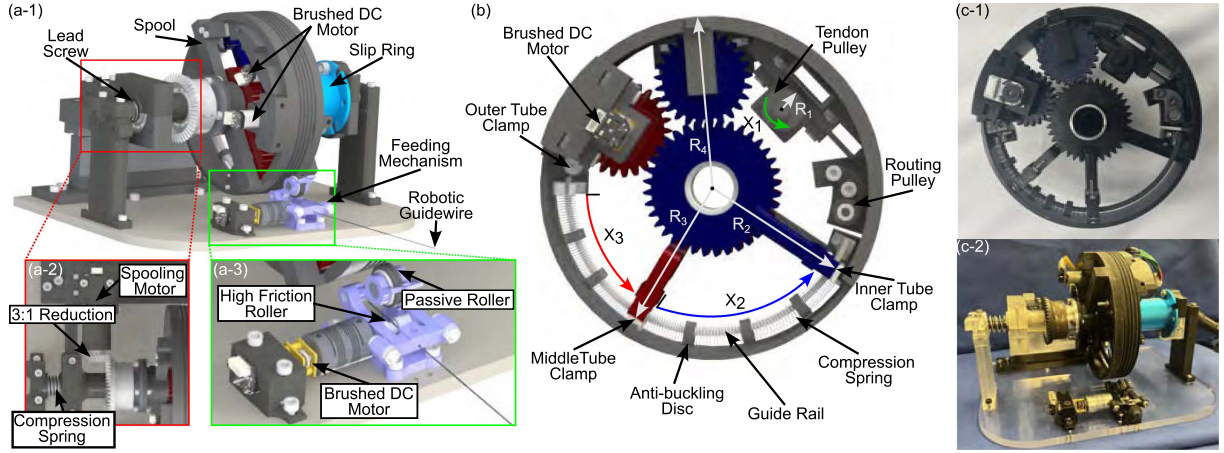


Fig. 2. A schematic of (a-1) the compact spooling mechanism for the COAST guidewire robot, (a-2) the spool rotation gear train, (a-3) the feeding mechanism, and (b) the internal actuation components of the spool. An image of the (c-1) spool with internal components and (c-2) completed spooling mechanism.

TABLE I  
SPECIFICATIONS OF THE COAST GUIDEWIRE

Items	Outer tube	Middle tube	Inner tube	Tendon
Total length (mm)	950	975	1000	1056.3
Notched length (mm)	112.8	75.0	-	-
Outer diameter (mm)	0.48	0.36	0.26	0.076
Inner diameter (mm)	0.40	0.30	0.19	-
Notch depth, $d$ (mm)	0.400	0.243	-	-
Notch width, $h$ (mm)	0.315	0.315	-	-
Notch spacing, $c$ (mm)	0.285	0.285	-	-
Number of notches, $N$	188	125	-	-
Young's Modulus, $E$ (Gpa)	42.7	42.7	42.7	34.8

be increased or decreased by retracting or inserting the inner tube, respectively. Lastly, the extended segment consists of only the outer tube that has been extended forward. This motion is termed extended-feed (ExF) motion and results in the outer tube translating on the tangent of the curve being held by the middle tube.

The compliance of the guidewire robot can be customized for a desired clinical task or procedure through the notch parameters of the UAN joint  $\{d, c, h\}$  where  $d$  is the notch depth,  $c$  is the notch spacing, and  $h$  is the notch width as shown in Fig. 1(b-1). In this work, the machining parameters,  $\{d, c, h\}$ , are selected to be  $\{0.243 \text{ mm}, 0.285 \text{ mm}, 0.315 \text{ mm}\}$  for middle tube and  $\{0.4 \text{ mm}, 0.285 \text{ mm}, 0.315 \text{ mm}\}$  for the outer tube. These parameters were chosen to minimize abrupt changes in the shape of the robot as a result of “snapping”, whereby there is an instantaneous change in the curvature of the robot. By selecting a sufficiently low flexural stiffness ratio [25] and allowing for sufficiently large deflections, such as those seen in the aortic bifurcation [29], we can minimize “snapping”. The cross-section of a laser micromachined tube is shown in Fig. 1(b-2) where  $r_i$  and  $r_o$  are the inner and outer radii of the tube, respectively, and  $\phi$  is the angle of the notched segment after being laser micromachined is given by:

$$\phi = 2 \arccos \left( \frac{d - r_o}{r_o} \right) \quad (1)$$

which results in the second moment of area about the x-axis given by:

$$I = \frac{(r_o^4 - r_i^4)(\phi + \sin \phi)}{8} - \frac{8 \sin^2(\frac{\phi}{2})(r_o^3 - r_i^3)^2}{9\phi(r_o^2 - r_i^2)} \quad (2)$$

The Young's modulus of the NiTi tubes are assumed to be the same and are given as approximately 42.7 GPa by the manufacturer. The micro-tendon has a Young's modulus of 34.8 GPa determined in [30]. A summary of the parameters for each component of the COAST guidewire robot is given in Table I and an image of the assembled COAST guidewire robot is shown in Fig. 1(c).

### B. Compact Spooling Mechanism

The compact spooling mechanism developed in this work is capable of housing 150 cm of the COAST guidewire robot with dimensions: 212 mm  $\times$  175 mm  $\times$  137 mm. The spooling mechanism, shown in Fig. 2(a-1) houses a 3D-printed (J35<sup>TM</sup>Pro, Stratasys, Ltd., MN, USA) cylindrical structure (the spool) with a radius of 60 mm and a helical groove (3 mm/rev pitch) for winding the COAST guidewire around. The length of guidewire capable of being housed is dependent on the number of revolutions of the helical groove. The spool rests on a lead screw with a 3 mm/rev pitch to facilitate translation while rotating the spool to ensure the outlet of the wire from the spool remains fixed relative to other components. The spool is rotated by a brushed DC motor with a 380:1 gear ratio (Pololu Robotics and Electronics, NV, United States) that meshes with a bevel gear attached to the spool with a 3:1 gear ratio. The DC motor is fixed to a translating arm that slides on a linear rail as the spooling mechanism translates on the lead screw that passes concentrically through the spool. A compression spring is utilized to ensure the spiral bevel gears remain in contact while in motion. The mechanism for rotating the spool is shown in Fig. 2(a-2). The feeding mechanism, shown in Fig. 2(a-3), ensures the guidewire is constrained and assists with spooling/unspooling the guidewire. The guidewire rests on a high friction roller, consisting of a rubber segment on a steel



shaft, and is held in place by a passive 3D printed roller (Projet 5600, 3D Systems, South Carolina, USA). The roller is actuated by a brushed DC motor (gear ratio 100:1). The velocity of the roller is synced with the velocity of the guidewire exiting the spool to prevent the guidewire from lifting off the helical groove of the spool.

The internal structure of the spool is shown in Fig. 2(b) and houses the components to translate the middle and inner tube of the COAST guidewire as well as those for actuating the tendon. The middle tube and inner tube are attached to their respective rotating arms that have an exterior spur gear assembly (gear ratio of 36:25) driven by brushed DC motors with a gear ratio of 380:1 and nominal torque of 110 mNm. The ends of these arms translate around a 3D-printed circular track with a groove for the tubes. To prevent buckling of the sub-mm tubes, 3D-printed anti-buckling discs are placed periodically throughout the guide rail with compression springs in between. These discs constrain the tubes to the guide rail, preventing buckling while translating the tubes. The tendon of the COAST guidewire robot is routed through a 3D-printed pulley to the tendon pulley (radius of 7.4 mm) which is driven by a brushed DC motor with a gear ratio of 380:1. The wires for the spooling mechanism motors are routed through the assembly to a slip ring (Senring, Shenzhen, China) which is connected to the translation arm, preventing any unwanted cable twisting or motion.

Unlike many other continuum robots, the COAST guidewire robot is capable of a variable bending length. This, in conjunction with tendon stroke and translation of the guidewire, enables follow-the-leader (FTL) motion. The guidewire can maintain a curve and translate the outer tube over the tip, resulting in pure translation along the tangent of the tip of the guidewire (ExF motion). Lastly, the entire spooling mechanism can be externally rotated to adjust the bending plane of the guidewire. The following control variables are introduced:

$$\begin{bmatrix} \psi \\ X_1 \\ X_2 \\ X_3 \\ X_4 \end{bmatrix} = \begin{bmatrix} \text{Roll of the Spooling Mechanism} \\ \text{Tendon Stroke} \\ \text{Bending Segment Length} \\ \text{Middle Tube Displacement} \\ \text{Guidewire Feed} \end{bmatrix}$$

The middle tube displacement,  $X_3$ , and the guidewire feed,  $X_4$ , are both given as lengths of tube deployed from the spooling mechanism. The roll of the spool can be enabled through an external device such as a rotating stage or a serial manipulator. Furthermore, the mechanism is sufficiently compact for potential adaptation into a held-held module. The primary difference between enabling these motions for this mechanism and our previous mechanism [28] is how the outer tube is translated. Previously the outer tube was translated while the middle tube was fixed, but in this case, it is the opposite. To extend the outer tube, the guidewire is unspooled and the internal components (middle tube, inner tube, and tendon stroke) are all equally retracted.

For a desired component motion,  $X_i$  where  $i \in \{1, 2, 3, 4\}$ , the motor rotation required to achieve that motion,  $\theta_i$ ,

is given by:

$$\theta_i = \frac{X_i}{N_m N_i R_i} \quad (3)$$

where  $N_m$  is the gear reduction of the motor,  $N_i$  is the gear reduction attached to the output shaft of the motor, and  $R_i$  is the radius of the pulley/arm attached to the gear as shown in Fig. 2(b). A picture of the interior of the spool is shown in Fig. 2(c-1) and the fully assembled spooling mechanism is shown in Fig. 2(c-2).

### C. Guidewire Kinematics

The kinematics of the guidewire relate the deflection of the bending joint to the tendon stroke,  $X_1$ . A common assumption that is utilized in this work is that the bending segment of the joint deflects with a constant curvature. While tissue interactions are integral to guidewire steering, several works have demonstrated success utilizing constant curvature models for steering the distal end of robotic guidewires and catheters [4], [27], [31], [32]. Our previous work, [9], has derived an expression for the kinematics of the COAST guidewire robot which includes a kinematic term,  $\Delta L^{kin}(\kappa, X_2)$  and tendon elongation. However, the combined tubes can have an initial pre-curvature,  $\kappa_0$ . The kinematics of the guidewire presented in this work maps the desired change in curvature to the tendon stroke required to do so, given by:

$$X_1 = \underbrace{\Delta L^{kin}(\kappa, X_2, \kappa_0)}_{\text{Kinematic term}} + \underbrace{\eta^{N_f} f(X_1, X_2, X_3, X_4)}_{\text{Friction}} \underbrace{\frac{E(I_{out} + I_{mid})L_t(\kappa - \kappa_0)}{\Delta y_t E_t \pi r_t^2}}_{\text{Tendon Elongation}} \quad (4)$$

where  $E$  is the Young's modulus of the nitinol tubes,  $E_t$  is the Young's modulus of the tendon,  $r_t$  is the tendon radius,  $L_t$  is the length of the tendon,  $I_{out}$  and  $I_{mid}$  are the second moment of area of the outer and middle tubes (given by (2)), respectively, and  $\Delta y$  is the moment arm for an applied tendon force given by:

$$\Delta y = \bar{y}_{mid} + r_{i,mid} - r_t = \frac{4 \sin \frac{\phi_{mid}}{2} (r_{o,mid}^3 - r_{i,mid}^3)}{3\phi(r_{o,mid}^2 - r_{i,mid}^2)} + r_{i,mid} - r_t \quad (5)$$

where  $\bar{y}_{mid}$  is the y coordinate of the neutral axis of the middle tube relative to the geometric center. The kinematic term,  $\Delta L^{kin}(\kappa, X_2, \kappa_0)$  is the difference in the tendon stroke between the pre-curved shape and the desired curvature is given by [28]:

$$\Delta L^{kin}(\kappa, X_2, \kappa_0) = L_i(\kappa_0, X_2) - (L_{cur}(\kappa) + L_{str}(\kappa)) \quad (6)$$

where  $L_i(\kappa_0, X_2)$  is the initial length of the tendon in the pre-curved segment,  $L_{cur}(\kappa)$  is the tendon arc length in curved section, and  $L_{str}(\kappa)$  is the length of the tendon in straight between the inner and middle tubes as indicated in Fig. 3.

Additionally, friction in the system contributes significantly to the elongation of the tendon. One source of friction is due to the friction between the notches and tendon, given by  $\eta^{N_f}$ ,

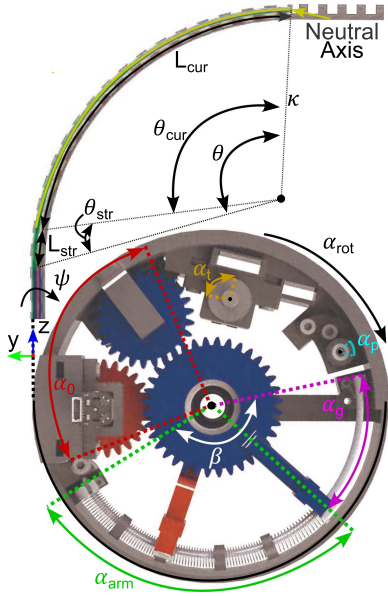


Fig. 3. A schematic showing the guidewire joint kinematics for a given curvature and the capstan friction components in the spool.

where  $\eta$  is the coefficient of friction and  $N_f = X_2 N_{mid} / L_{mid}^{notch}$ , where  $L_{mid}^{notch}$  is the notched length of the middle tube, are the number of notch interactions. Additionally, a capstan friction component  $f(X_1, X_2, X_3, X_4)$  is the result of the wrapping of each component around the spool, pulley, or guide rail. The tendon contacts several components within the mechanism including throughout the inner tube, on the plastic guide rail, and on the tendon pulleys. The wrapping angle on the outside of the spool,  $\alpha_{rot}(X_4)$ , is given by:

$$\alpha_{rot}(X_4) = \frac{L - X_4}{R_4} \quad (7)$$

where  $L$  is the total length of the guidewire contained within the spool and  $R_4$  is the radius of the spool. The constant arc between the armatures and the spool entrance has wrapping angle  $\alpha_0$  and the section of the guide rail contacting the inner tube due to arm actuation,  $\alpha_{arm}(X_2, X_3)$ , is given by:

$$\alpha_{arm}(X_2, X_3) = \frac{X_3}{R_3} + \frac{X_2}{R_2} + \alpha_{X_{3,0}} + \alpha_{X_{2,0}} \quad (8)$$

where  $\alpha_{X_{3,0}}$  and  $\alpha_{X_{2,0}}$  are the angles created by the spacers in the unactuated positions of  $X_2$  and  $X_3$ , respectively,  $R_2$  is the inner tube arm length, and  $R_3$  is the middle tube arm length. The contact angle along the guide rail,  $\alpha_g$ , is given by:

$$\alpha_g(X_2, X_3) = \beta - \alpha_{arm}(X_2, X_3) \quad (9)$$

where  $\beta$  is the constant arc of the entire guide rail. Lastly, the tendon contacts the constant tendon pulley contact angle  $\alpha_p$  and the wrapping angle caused by the tendon stroke,  $\alpha_t(X_1)$ , is given by:

$$\alpha_t(X_1) = \frac{X_1}{R_1} \quad (10)$$

Each contact angle is shown in Fig. 3. The coefficient of friction for the tendon pulleys, nitinol tubes, and guide rail are given by

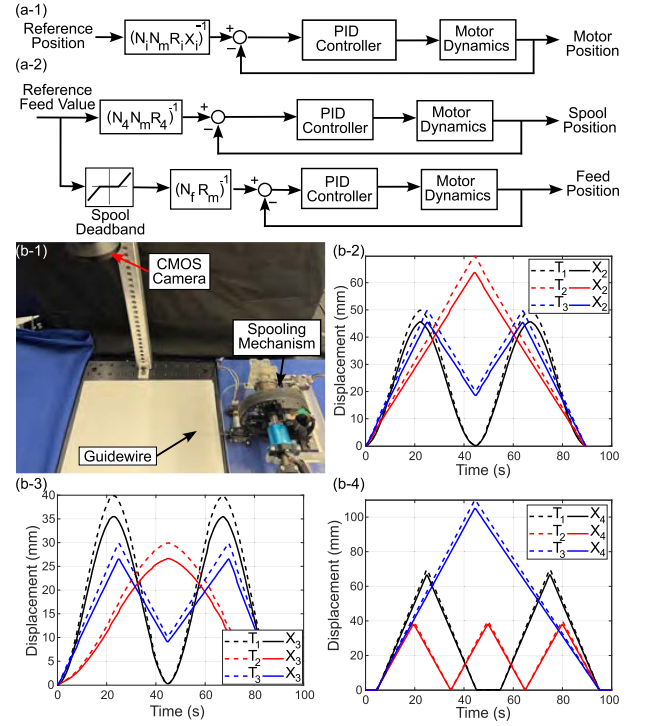


Fig. 4. Schematic showing the control scheme for (a-1) each internal component of the spool and (a-2) the coupled spooling and feeding mechanism. The (b-1) experimental setup for calibration and validation of the translation of (b-2) the inner tube, (b-3) the middle tube, and (b-4) the outer tube using the calibrated spool parameters.

$\mu_t, \mu_{in}$ , and  $\mu_g$ , respectively, and are experimentally determined in Section III-B. The full expression for the capstan component of friction is given by:

$$f(X_1, X_2, X_3, X_4) = \underbrace{e^{\mu_{in}[\alpha_0 + \alpha_{rot}(X_4) + \alpha_{arm}(X_2, X_3)]}}_{\text{NiTi Contact}} \underbrace{e^{\mu_t[\alpha_t(X_1) + \alpha_p] + \mu_g \alpha_g(X_2, X_3)}}_{\text{Mechanism Contact}} \quad (11)$$

As a result, the tendon stroke required to achieve a desired curvature is expected to increase as the guidewire is spooled or as the bending length increases. This model is experimentally validated in Section III-B.

### III. EXPERIMENTS AND RESULTS

#### A. Mechanism Calibration and Control

To validate the motion of each component of the mechanism, the individual guidewire components (inner tube, middle tube, outer tube) were isolated and attached to the mechanism. The components were given several reference trajectories and translated on a level surface with a PTFE tube at the back end to reduce friction while translating. The tendon stroke, inner tube, and middle tube displacements utilize the control scheme shown in Fig. 4(a-1). However, due to the need to synchronize the feeding motor and the rotation of the spool, the inputs are coupled using the control scheme shown in Fig. 4(a-2), including the backlash present in the spooling rotation through a simple deadband model with a dead zone of approximately 0.4 rd.

TABLE II  
CALIBRATED PARAMETERS AND THE RMSE FOR EACH TRAJECTORY  
FOLLOWED BY EACH INTERNAL COMPONENT OF THE COMPACT SPOILING  
MECHANISM

Component	Calibrated Radius (mm)	RMSE (mm)		
		$T_1$	$T_2$	$T_3$
Inner Tube, $X_2$	48.07	2.58	3.43	2.77
Middle Tube, $X_3$	47.80	2.65	1.97	2.09
Feed, $X_4$	61.30	1.58	0.96	2.63

Each motor position reference is then passed to a PID controller using an encoder for position feedback. Each control scheme was executed in Simulink Desktop Real-Time (Simulink 2022b, MathWorks Inc., Natick, MA, USA) at a frequency of 500 Hz. To validate the motion of each component, a CMOS camera (Zelux<sup>TM</sup> 1.6 MP, Thorlabs Inc., NJ, United States) captured images from above during each trajectory. The displacement of the guidewire was tracked by segmenting the image and recording the displacement of the pixels at the tip (1 pixel = 0.14 mm). The experimental setup for calibration is shown in Fig. 4(b-1).

While component measurements from the manufacturing drawings can be utilized to extract system parameters, manufacturing errors can lead to sub-optimal tracking performance. Therefore, calibration of the internal components of the spooling mechanism is required to ensure precise displacement of each tube and the tendon. For this reason, several trajectories were utilized to calibrate the radius of each armature and the spool. There were a total of 8 different reference trajectories used to calibrate the components of the spooling mechanism. The radius of the spooling mechanism,  $R_4$ , the middle tube arm,  $R_3$ , and the inner tube arm,  $R_2$ , were calibrated by minimizing the error norm, computed by the difference in the reference trajectories and predicted motion using (3) for each component. Since the spool rotation determines how much wire is released, the radius of the spool is the only component calibrated for the feed of the guidewire. The calibrated values for the inner tube, middle tube, and feed displacement radii are shown in Table II. Additionally, the tracking performance using the calibrated parameters for three reference trajectories  $\{T_1, T_2, T_3\}$  for the inner tube, middle tube, and feed displacement is shown in Fig. 4(b-2), (b-3), and (b-4), respectively, with RMSE values for each trajectory shown in Table II.

The average RMSE for the three trajectories presented are 2.93 mm, 2.24 mm, and 1.72 mm for  $X_2$ ,  $X_3$ , and  $X_4$ , respectively, showing sufficient accuracy for steering the guidewire robot. Increased errors in the retraction/insertion of the inner tube and middle tube are attributed to deviations from the semi-circular guide rail path when being actuated. This is hypothesized to be resulting from the clearance between the NiTi tubes, the anti-buckling disks, and the guide rail. For this reason, the inner tube has the largest RMSE as it traverses the most along the guide rail.

### B. Guidewire Kinematics Validation

To validate the mechanics of the guidewire presented in Section II-C, the guidewire was imaged under a CMOS camera to capture the curvature changes when applying a tendon stroke,  $X_1$ , in different configurations of  $X_2$ ,  $X_3$ , and  $X_4$ . To capture

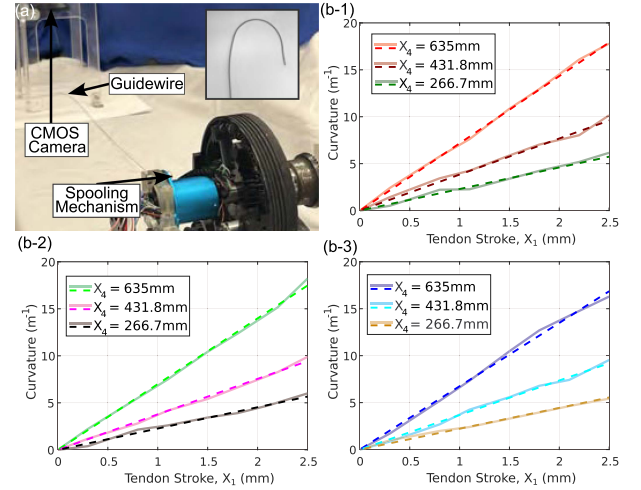


Fig. 5. (a) An image of the bending characterization experimental setup with (a)(inset) an example image of the guidewire bending. Plots of tendon stroke vs curvature for bending lengths ( $X_2$ ) of (b-1) 25 mm, (b-2) 35 mm, and (b-3) 50 mm showing measured data (solid lines) and the kinematics model (dashed lines) for different spooled lengths ( $X_4$ ).

TABLE III  
RMSE IN  $m^{-1}$  BETWEEN THE MEASURED DATA AND THE KINEMATIC MODEL

		$X_4$ (mm)		
		635.0	431.8	266.7
$X_2$ (mm)	25	0.187	0.302	0.237
	35	0.300	0.212	0.211
	50	0.339	0.228	0.144

the curvature, the image of the guidewire, an example shown in Fig. 5(a)(inset) was first passed through a Frangi filter [33] and then binarized to segment the guidewire from the background. Pratt's method [34] was used to fit a circular arc to the curved segment of the guidewire to characterize the deflection. The coefficients of friction are tuned manually with initial guesses from our previous work [28], using calibration data sets for bending lengths of 20 mm, 40 mm, and 60 mm at varying spool lengths ranging from 200 mm to 400 mm. The coefficients of friction were determined to be  $\eta = 1.3$ ,  $\mu_{in} = 0.19$ ,  $\mu_g = 0.26$ , and  $\mu_t = 0.29$ .

The experimental curvature and modeled curvature from the tendon stroke is shown in Fig. 5(b-1), (b-2), and (b-3) for bending lengths of 25 mm, 35 mm, and 50 mm, respectively, for  $X_4$  values of 635.0 mm, 431.8 mm, and 266.7 mm. The maximum curvature achieved was  $17.79 m^{-1}$ ,  $18.21 m^{-1}$ , and  $16.30 m^{-1}$  for bending lengths of 25 mm, 35 mm, and 50 mm, respectively. The model and data indicate that the capstan component of friction from the guidewire being spooled dominates the kinematics as the guidewire becomes increasingly spooled. The RMSE of the measured curvature and the theoretical curvature computed from the tendon stroke is shown in Table III for the varying bending lengths and spooled lengths. The average RMSE for all of the data shown is  $0.24 m^{-1}$  with the largest RMSE being  $0.339 m^{-1}$  which is considered sufficient for enabling teleoperated control of the COAST guidewire robot which will be considered for our future works for *ex vivo* and *in vivo* testing using the spooling mechanism.



#### IV. CONCLUSION

The work presented in this letter details a novel and highly compact actuation mechanism for the sub-mm COAST guidewire robot at clinically viable lengths up to 150 cm. Validation and testing of the mechanism show sufficient performance in actuating the components of the COAST guidewire robot with average trajectory RMSE values of 2.93 mm, 2.24 mm, and 1.72 mm for the inner tube, middle tube, and feeding mechanism, respectively. Additionally, the kinematics of the robotic guidewire, including friction and kinematic components from the compact spooling mechanism, show sufficient performance for mapping the tendon stroke to curvature with average RMSE values of  $0.24 \text{ m}^{-1}$  for a variety of bending lengths and spooled lengths. Future work will focus on including the effects of external forces in the bending model and enabling feedback control of the guidewire through imaging or shape sensing. Furthermore, *ex vivo* and *in vivo* traversal experiments are planned to fully evaluate the clinical feasibility of the proposed mechanism and the COAST guidewire robot.

#### REFERENCES

- [1] "Cardiovascular diseases (CVDs)" Who.int. Accessed: May 30, 2023. [Online]. Available: [https://www.who.int/en/news-room/fact-sheets/detail/cardiovascular-diseases-\(cvds\)](https://www.who.int/en/news-room/fact-sheets/detail/cardiovascular-diseases-(cvds))
- [2] S. S. Virani et al., "Heart disease and stroke statistics—2021 update: A report from the american heart association," *Circulation*, vol. 143, no. 8, pp. e254–e743, 2021.
- [3] A. Abdalwahab, M. Farag, E. S. Brilakis, A. R. Galassi, and M. Eged, "Management of coronary artery perforation," *Cardiovasc. Revascularization Med.*, vol. 26, pp. 55–60, 2021.
- [4] S. R. Ravigopal, T. A. Brumfiel, A. Sarma, and J. P. Desai, "Fluoroscopic image-based 3-D environment reconstruction and automated path planning for a robotically steerable guidewire," *IEEE Robot. Automat. Lett.*, vol. 7, no. 4, pp. 11918–11925, Oct. 2022.
- [5] N. J. Deaton, T. A. Brumfiel, A. Sarma, and J. P. Desai, "Simultaneous shape and tip force sensing for the COAST guidewire robot," *IEEE Robot. Automat. Lett.*, vol. 8, no. 6, pp. 3725–3731, Jun. 2023.
- [6] V. Aloï, K. T. Dang, E. J. Barth, and C. Rucker, "Estimating forces along continuum robots," *IEEE Robot. Automat. Lett.*, vol. 7, no. 4, pp. 8877–8884, Oct. 2022.
- [7] T. A. Brumfiel, A. Sarma, and J. P. Desai, "Towards FBG-based end-effector force estimation for a steerable continuum robot," in *2022 Int. Symp. Med. Robot.*, 2022, pp. 1–7.
- [8] T. A. Brumfiel, R. Qi, S. Ravigopal, and J. P. Desai, "Image-based force localization and estimation of a micro-scale continuum guidewire robot," *IEEE Trans. Med. Robot. Bionics*, vol. 6, no. 1, pp. 153–162, Feb. 2024.
- [9] A. Sarma, T. A. Brumfiel, Y. Chitalia, and J. P. Desai, "Kinematic modeling and Jacobian-based control of the COAST guidewire robot," *IEEE Trans. Med. Robot. Bionics*, vol. 4, no. 4, pp. 967–975, Nov. 2022.
- [10] Y. Chitalia, X. Wang, and J. P. Desai, "Design, modeling and control of a 2-DoF robotic guidewire," in *2018 IEEE Int. Conf. Robot. Automat.*, 2018, pp. 32–37.
- [11] T.-D. Nguyen and J. Burgner-Kahrs, "A tendon-driven continuum robot with extensible sections," in *2015 IEEE/RSJ Int. Conf. Intell. Robots Syst.*, 2015, pp. 2130–2135.
- [12] S. Jeon et al., "A magnetically controlled soft microrobot steering a guidewire in a three-dimensional phantom vascular network," *Soft Robot.*, vol. 6, no. 1, pp. 54–68, 2019.
- [13] J. Kim, P. B. Nguyen, B. Kang, E. Choi, J.-O. Park, and C.-S. Kim, "A novel tip-positioning control of a magnetically steerable guidewire in sharply curved blood vessel for percutaneous coronary intervention," *Int. J. Control, Automat. Syst.*, vol. 17, no. 8, pp. 2069–2082, 2019.
- [14] Z. Yang, H. Yang, Y. Cao, Y. Cui, and L. Zhang, "Magnetically actuated continuum medical robots: A review," *Adv. Intell. Syst.*, vol. 5, 2023, Art. no. 2200416, doi: [10.1002/aisy.202200416](https://doi.org/10.1002/aisy.202200416).
- [15] H. Alfalahi, F. Renda, and C. Stefanini, "Concentric tube robots for minimally invasive surgery: Current applications and future opportunities," *IEEE Trans. Med. Robot. Bionics*, vol. 2, no. 3, pp. 410–424, Aug. 2020.
- [16] J. Till et al., "A dynamic model for concentric tube robots," *IEEE Trans. Robot.*, vol. 36, no. 6, pp. 1704–1718, Dec. 2020.
- [17] J. Ha and P. E. Dupont, "Incorporating tube-to-tube clearances in the kinematics of concentric tube robots," in *2017 IEEE Int. Conf. Robot. Automat.*, 2017, pp. 6730–6736.
- [18] A. L. Gunderman et al., "Non-metallic MR-Guided concentric tube robot for intracerebral hemorrhage evacuation," *IEEE Trans. Biomed. Eng.*, vol. 70, no. 10, pp. 2895–2904, Oct. 2023.
- [19] M. Ho, A. B. McMillan, J. M. Simard, R. Gullapalli, and J. P. Desai, "Toward a meso-scale SMA-actuated MRI-compatible neurosurgical robot," *IEEE Trans. Robot.*, vol. 28, no. 1, pp. 213–222, Feb. 2012.
- [20] Y. Goergen et al., "Modular design of an SMA driven continuum robot," *Smart Mater., Adaptive Struct. Intell. Syst., Amer. Soc. Mech. Eng.*, vol. 84027, 2020.
- [21] M. P. Kummer, J. J. Abbott, B. E. Kratochvil, R. Borer, A. Sengul, and B. J. Nelson, "OctoMag: An electromagnetic system for 5-DoF wireless micromanipulation," *IEEE Trans. Robot.*, vol. 26, no. 6, pp. 1006–1017, Dec. 2010.
- [22] Y. Lu, K. Mani, B. Panigrahi, S. Hajari, and C. Chen, "A shape memory alloy-based miniaturized actuator for catheter interventions," *Cardiovasc. Eng. Technol.*, vol. 9, pp. 405–413, 2018.
- [23] Q. Ding, J. Chen, W. Yan, K. Yan, A. Kyme, and S. S. Cheng, "A high-performance modular SMA actuator with fast heating and active cooling for medical robotics," *IEEE/ASME Trans. Mechatron.*, vol. 27, no. 6, pp. 5902–5913, Dec. 2022.
- [24] C. Girerd and T. K. Morimoto, "Design and control of a hand-held concentric tube robot for minimally invasive surgery," *IEEE Trans. Robot.*, vol. 37, no. 4, pp. 1022–1038, Aug. 2021.
- [25] Y. Chitalia, A. Sarma, T. A. Brumfiel, N. J. Deaton, M. Sheft, and J. P. Desai, "Model-based design of the COAST guidewire robot for large deflection," *IEEE Robot. Automat. Lett.*, vol. 8, no. 9, pp. 5345–5352, Sep. 2023.
- [26] S. Jeong, Y. Chitalia, and J. P. Desai, "Design, modeling, and control of a coaxially aligned steerable (COAST) guidewire robot," *IEEE Robot. Automat. Lett.*, vol. 5, no. 3, pp. 4947–4954, Jul. 2020.
- [27] S. R. Ravigopal, T. A. Brumfiel, and J. P. Desai, "Automated motion control of the COAST robotic guidewire under fluoroscopic guidance," in *2021 Int. Symp. Med. Robot.*, 2021, pp. 1–7.
- [28] P. Lis, A. Sarma, G. Trimpe, T. A. Brumfiel, R. Qi, and J. P. Desai, "Design and modeling of a compact advancement mechanism for a modified COAST guidewire robot," in *2022 Int. Conf. Robot. Automat.*, 2022, pp. 1176–1182.
- [29] C. Barger et al., "Distribution of the geometric parameters of human aortic bifurcations," *Arteriosclerosis: Official J. Amer. Heart Assoc., Inc.*, vol. 6, no. 1, pp. 109–113, 1986.
- [30] T. A. Brumfiel et al., "Design and modeling of a sub-2 mm steerable neuroendoscopic grasping tool," *IEEE Trans. Med. Robot. Bionics*, vol. 5, no. 4, pp. 1105–1109, Nov. 2023.
- [31] S. Fu et al., "A magnetically controlled guidewire robot system with steering and propulsion capabilities for vascular interventional surgery," *Adv. Intell. Syst.*, vol. 5, no. 11, 2023, Art. no. 2300267.
- [32] R. Qi, N. U. Nayar, and J. P. Jaydev, "Telerobotic transcatheter delivery system for mitral valve implant," *IEEE Robot. Automat. Lett.*, vol. 8, no. 6, pp. 3629–3636, Jun. 2023.
- [33] A. F. Frangi, W. J. Niessen, K. L. Vincken, and M. A. Viergever, "Multiscale vessel enhancement filtering," in *Proc. Med. Image Comput. Comput.- Assist. Intervention-MICCAI-98: 1st Int. Conf.*, Cambridge, MA, USA, 1998, pp. 130–137.
- [34] V. Pratt, "Direct least-squares fitting of algebraic surfaces," *ACM SIG-GRAPH Comput. Graph.*, vol. 21, no. 4, pp. 145–152, 1987.